

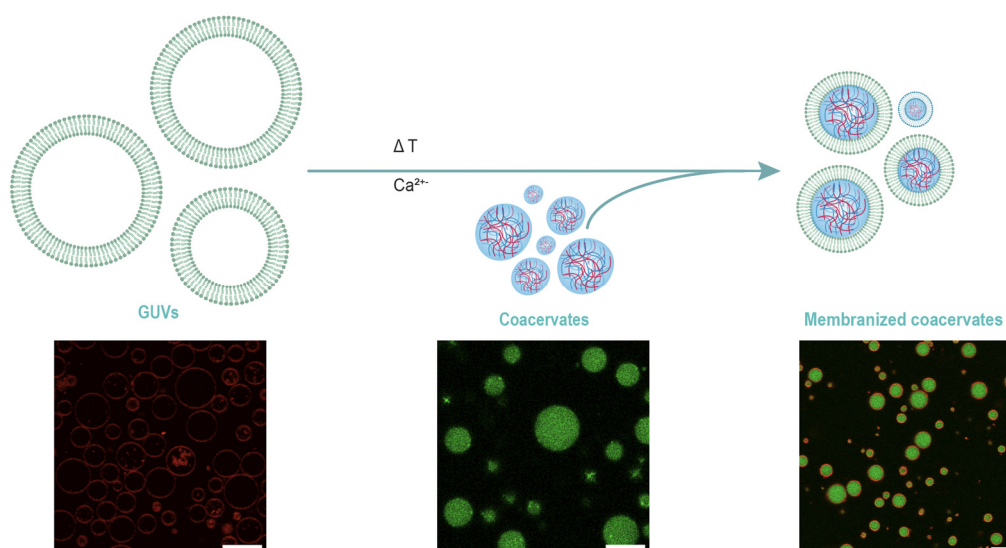
1 **Spontaneous wrapping of coacervates by lipid bilayers upon heat shock creates**
2 **resilient and intact membranized coacervates**

3 Sadaf Javed¹, Evan Spruijt*¹

4
5 ¹*Institute for Molecules and Materials, Radboud University, Heyendaalseweg 135, 6523 AJ Nijmegen,*
6 *The Netherlands.* * E-mail: e.spruijt@science.ru.nl

7
8 **Abstract**

9 Membranes and membraneless biocondensates help organize cells and work synergistically to drive
10 cellular processes. Separately, membrane-bound and membraneless compartments face difficulties as
11 stable protocells or synthetic cell systems. Here, we present a new method to create membranized
12 coacervates (MCs) for coacervates with any surface charge and a wide range of phospholipid membrane
13 compositions. MCs are formed when liposomes, destabilized using heat and divalent ions, are mixed with
14 coacervate dispersions. Unlike previous reports of hybrid coacervates surrounded by membranes, the MC
15 membranes form an effective barrier also against small molecules, including calcein and TAMRA, The MC
16 membranes provide excellent stability to the protocells at pH 3-11, salt concentrations up to 0.5 M,
17 hypotonic and hypertonic conditions, and repeated freeze-thaw cycles. MCs performed better in all the
18 tested conditions than both coacervates and liposomes. We ascribe this behavior to the increased stability
19 that coacervates and liposomes confer to each other when together. MC membranes are fluid, allowing
20 lateral lipid diffusion, but the lipids are more densely packed compared to their corresponding liposomes.
21 MCs can help us understand how stable primitive cells might have formed, and help us build advanced
22 synthetic cells with enhanced stability and selectivity.



23

24 1. Introduction

25

26 An integral feature of all living matter is the boundary that exists between the internal and the external
27 environments. In modern-day cells, the cell membrane, composed of a lipid bilayer, is a well-known
28 example of such a boundary. Apart from membranes, subcellular compartments, such as biomolecular
29 condensates, help create distinct chemical environments within the cell cytoplasm. Biomolecular
30 condensates are dense, biomolecule-rich structures formed via liquid-liquid phase separation (LLPS) of
31 molecules that lack the classic membrane boundary. Nonetheless, the liquid-liquid interface between
32 biomolecular condensates and the intracellular or intranuclear medium plays a central role in regulating
33 processes, such as, ribosome biogenesis [1] and cellular stress response [2]. Recent evidence indicates
34 that membranes and biocondensates work synergistically to drive crucial processes, such as mRNA
35 transport [3], signal transduction in T cells [4], and autophagy and membrane repair [5].

36 Compartmentalization must have also been a crucial requirement for the persistence and
37 subsequent evolution of early cells, often referred to as protocells. While membrane-based vesicles and
38 membrane-free coacervates have both been considered as protocell models, each has its own limitations.
39 Liposomes form a selective barrier between the inside and outside but fail to encapsulate high
40 concentrations of biomolecules in their lumen. They are also prone to bursting or collapsing under
41 osmotic stress. Coacervates, on the other hand, efficiently sequester biomolecules at high concentrations
42 [6], but are prone to coalescence and wetting and are sensitive to fluctuations in pH, temperature, and/or
43 salt concentrations. However, different primitive cell-like entities could have emerged simultaneously
44 through separate processes [7-10], manifesting as diverse structures, some closer to condensates while
45 others akin to membranous vesicles. Interactions between clusters of such structures could have led to
46 more complex assemblies, exhibiting a wider range of functions. Ultimately, integrating liposomes and
47 coacervates in one symbiotic system can lead to stable and functional protocells capable of delivering and
48 exchanging molecules across membranes.

49 Studies on biocondensate and membrane interactions in cells have shown that structures
50 comprising the two can be formed without compromising the essential features of the individual
51 components [11]. Lu et al. demonstrated that coacervates can wet liposomal membranes to varying
52 degrees and can enter the vesicle lumen via an endocytosis-like process [12]. Both compartments can
53 remodel each other, often resulting in complex morphologies, such as ruffled or deformed membranes
54 and spreading coacervates [13]. As they interact, coacervates modulate the packing of lipids and their
55 hydration at the coacervate-membrane junction [14]. Coacervate-membrane interactions are partly
56 based on the ζ -potentials of coacervates and liposomes and the partitioning coefficients (K_d) of lipids into
57 the coacervates [15]. The greater the ζ -potential difference between the coacervate and the membrane,
58 the stronger is the interaction between the two. A larger K_d of the lipids can result in the coacervate

59 penetrating the membrane by taking up the lipids present at the coacervate-membrane junction.
60 However, manipulating these interactions to get complex, hierarchical structures remains a challenge.

61 Attempts have been made to create coacervate-phospholipid vesicle hybrid protocells [16,17].
62 However, only a little more than half of the coacervates in such cases have continuous membranes with
63 selective permeability that can keep smaller molecules out, and one third of the coacervates had
64 membranes with such large defects that oligonucleotides (U15) could pass [17]. The permeability in such
65 systems depends heavily on the partition coefficient of the client molecule into the coacervate, with a high
66 K_d favoring increased membrane permeability [18], making the membranes prone to leakage. Moreover,
67 the current methods to create phospholipid-coated coacervates only work for few coacervate and
68 membrane compositions, typically with opposite charge on the coacervates and the membranes, restricting
69 their applicability.

70 Here we present a simple and quick method to create phospholipid membrane-coated
71 coacervates with a wide range of complex coacervate systems and membrane compositions that is not
72 limited to oppositely charged coacervate-liposome combinations. When giant unilamellar vesicles (GUVs)
73 are destabilized by a brief heat shock in the presence of divalent ions, they become susceptible to
74 spreading onto surfaces. When they are mixed with coacervates upon cooling, they wrap around the
75 coacervates, forming membranized coacervates (MCs) with intact membranes. We postulate that this
76 wrapping of the liposomal membrane is a bid to stabilize the fissuring liposome using the coacervate as a
77 stabilizing surface, analogous to the spreading of GUV membranes on solid surfaces in the presence of
78 divalent ions [19]. We show that the method works for multiple coacervate and membrane compositions,
79 including neutral coacervates and liposomes, and even similarly charged coacervates and liposomes,
80 which otherwise do not interact with each other. The membranes around the MCs were continuous and
81 sufficiently defect-free to keep small molecules, such as calcein and TAMRA out of the inner coacervate,
82 despite their strong tendency to partition into the bare coacervates. Moreover, the MCs exhibited
83 significantly increased stability compared to both bare coacervates and empty GUVs under changing
84 environmental conditions, such as osmotic shocks and pH fluctuations.

85 These MCs, with their biomolecule-rich interior demarcated by a lipid membrane make versatile
86 protocell models. Owing to their increased resilience towards environmental changes, they can be used
87 to study protocell interactions over a wide range of conditions for longer durations compared with the
88 previously reported systems. Moreover, MCs can make efficient delivery vehicles as they sequester high
89 concentrations of molecules and are much more stable than both liposomes and coacervates alone.

90 2. Experimental Section

91

92 3.1 Lipids

93 All unlabelled lipids were purchased from Avanti Polar Lipids dissolved in chloroform (25 mg/mL). The
94 chloroform was evaporated, and the lipids were redissolved in half of the initial volume of chloroform to
95 obtain 50 mg/mL lipid stock solutions. The stock solutions were stored at -20 °C until use. 1,2-Dioleoyl-
96 *sn*-glycero-3-phosphoethanolamine (DOPE) conjugated to ATTO665 or ATTO633 was purchased from
97 ATTO-TEC GmbH in powder form and used to label the GUVs. The powder was dissolved in an appropriate
98 volume of chloroform to form 1 mg/mL stocks of the labeled lipids.

99

100 3.2 Coacervate components

101 K₁₀₀, E₁₀₀, R₃₀, and R₁₀ were purchased from Alamanda Polymers and dissolved in MQ at stock
102 concentrations of 50 mg/mL, 50 mg/mL, 0.10 M [monomer], and 0.10 M [monomer], respectively.
103 Hexametaphosphate, poly(diallyldimethylammonium chloride) (PDDA), ATP, and polyuridylic acid
104 (potassium salt) were purchased from Sigma Aldrich and dissolved in MQ at stock concentrations of 50
105 mg/mL, 50 mg/mL, 50 mM, 10 mg/mL, respectively. (RGRGG)₅ was purchased from Genscript and
106 dissolved in MQ at stock concentration of 0.10 M [monomer].

107

108 3.3 Coacervate formation

109 Coacervates were made by depositing the polycation and polyanion solutions on the wall of the
110 Eppendorf tube, containing Milli-Q, close to the meniscus. The final volume of the solution was 20 µL.
111 The tube was then vortexed, introducing the polymers in water to form coacervates in solution with the
112 desired final concentrations.

113

114 3.4 GUV formation

115 GUVs were created using the emulsion-transfer method [20]. Briefly, a total of 12 µL of lipid stock
116 solutions (final lipid concentration 1.5 mg/mL) were added in paraffin oil. Cholesterol was added at a final
117 concentration of 10 wt% or 20 wt% (relative to the lipids), and DOPE-PE and ATTO-DOPE labels were
118 added at a final concentration of 0.17 wt% (relative to the lipids). The final volume of the lipid mixture
119 was 400 µL. The mixture was heated at 80 °C on a thermoshaker for 5 minutes to evaporate the
120 chloroform under constant nitrogen gas flow to reduce the effects of humidity on the liposome formation.
121 Then, the oil-lipid mixture was sonicated for 15 mins in a bath sonicator. To make the emulsion, sucrose
122 was added to oil-lipid mixture to a final concentration of 300 mM and the tubes were agitated. After
123 incubating the emulsion for 10 mins, we layered it over 400 µL of 300 mM glucose in another tube. These
124 tubes were then centrifuged at 9000 rcf at 4 °C for 30 minutes. After centrifugation, the bottom of the

125 tubes were punctured using a needle and the pellets deposited in the aqueous phase were collected into
126 new tubes. The transferred suspension was centrifuged again at 6000 rcf at 4 °C for 10 minutes. The
127 supernatant was removed from the tubes and the pellet was resuspended in fresh 300 mM glucose. The
128 GUVs were then visualized under a confocal microscope.

129

130 *3.5 MC formation*

131 To make the MCs, we first added the appropriate divalent salt at a final concentration of 2 mM to the GUV
132 solution in a tube. Then, we make the coacervate solution by mixing the polycation and polyanion in MQ.
133 The GUV solution is then placed on a thermoshaker and heated at 60 °C for about a minute. We let the GUV
134 solution to cool down for 5-10 s before adding in the coacervate solution. Alternatively, we can also place
135 the tube containing the GUV solution on ice and immediately add the coacervate solution to it. The GUV-
136 coacervate mixture is then vortexed thoroughly for 30 s. The obtained MCs can be then visualized under a
137 microscope and used as desired.

138

139 *3.6 Membrane permeability assays*

140 After preparing the MCs, we added 20 µL each of the GUV, coacervate, and MC solutions in separate wells
141 of 18-flat well µSlide (Ibidi). Then, calcein was added at a final concentration of 2 mM in each well. For
142 K₁₀₀/pPhos coacervates and the corresponding MCs, 2 mM of 5-TAMRA was used to test the membrane
143 permeability instead of calcein. The samples were allowed to rest for 10 mins before imaging. For all
144 samples, we measured the average fluorescence intensities of five circular ROIs (area = 0.34 µm²) inside
145 the GUVs, coacervates, or MCs and in the solution to obtain the ratios of fluorescence intensity in/out.

146

147 *3.7 Image acquisition*

148 All confocal images were captured using a Leica SP8x confocal inverted microscope equipped with a DMI8
149 CS motorized stage, a pulsed white light laser, two HyD SP GaAsP and two PMT detectors. Images were
150 recorded using a 63x HC PL APO oil immersion objective.

151

152 *3.8 FRAP*

153 FRAP experiments were performed using a Leica SP8 SMD microscope with a HCX PL APO CS 63.0x1.20
154 WATER UV objective. We used a constant ROI area of 0.34 µm² for all measurements. The same area was
155 used to measure the control and background regions. The duration between each image acquisition was
156 3 s for all measurements. The membrane was labelled with ATTO633-DOPE. We recorded 20 frames
157 before bleaching the ROI. The ROI was bleached with 10 pulses of 544 nm argon laser at 100% intensity
158 and 50% power, and the recovery was monitored using 633 nm excitation laser at 0.5% intensity (50%
159 power) and the fluorescence detected using a PMT detector in the range of 645-670 nm.

160 The fluorescence intensities were normalized using the following formula [21]:

$$161 \quad F(t)_{norm} = 100 \times \frac{F(t)_{ROI} - F(t)_{bkgd}}{F(t)_{ctrl} - F(t)_{bkgd}} \times \frac{F(t)_{pre-ctrl} - F(t)_{bkgd}}{F(t)_{pre-ROI} - F(t)_{bkgd}}$$

162 Where, $F(t)_{ROI}$ is the fluorescence intensity of the ROI, $F(t)_{ctrl}$ is the fluorescence intensity of the
163 control region, $F(t)_{bkgd}$ is the fluorescence intensity in solution at time t, and $F(t)_{pre-ctrl}$ and
164 $F(t)_{pre-ROI}$ are the pre-bleach intensities of the control region and the ROI, respectively. The
165 fluorescence intensity recovery curve was fitted using FRAPbot (v. 1.9) [22] to obtain the $t_{1/2}$ values.

166

167 3.9 FLIM

168 FLIM imaging was performed using Leica SP8 SMD microscope equipped with a time-correlated single-
169 photon counting module from PicoQuant. The sample was excited using 488 nm pulsed argon laser
170 operating at 20 MHz, and the emission signal was collected using HyD detector from 550-650 nm in
171 photon counting mode. The fluorescence lifetime decay curves (for individual MCs and GUVs) were fitted
172 to a double-exponential model using FLIMfit [23]. The FliptR τ range was set from 2.5-7 ns and only pixels
173 falling in this range were included in the fit. Out of the two lifetime components, τ_1 was the longer
174 component with higher photon counts, and was used to represent the lifetime data.

175

176 3.10 Image analysis

177 Images were processed using ImageJ (FIJI). To count the number of MCs under different environmental
178 conditions and their size distribution, we used the EBImage package (Bioconductor) in R [24].

179

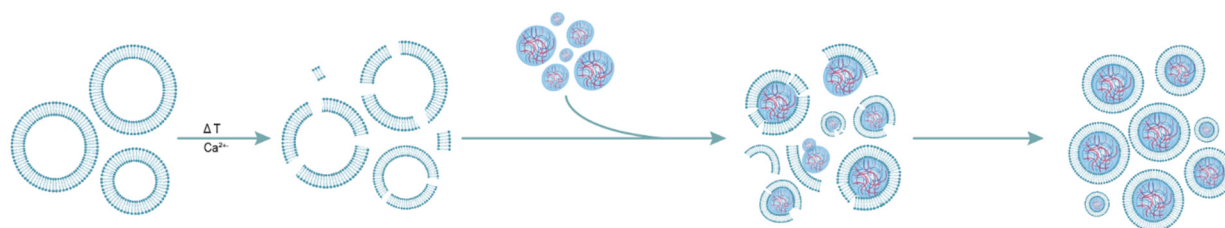
180 3. Results and discussion

181

182 3.1 A simple and robust method to create membranized coacervates

183 GUVs (1-100 μm in diameter) can be easily visualized under a microscope and are a good membrane
184 source for the MCs. Heating GUVs increases the kinetic energy of the constituent lipid molecules and
185 enhances membrane fluidity. Progressive increase in this kinetic energy, through an increase in
186 temperature and duration of heating, will ultimately result in the collapse of the lipid vesicle into an
187 aggregate. However, at temperatures below the tipping point, heating destabilizes the closed bilayer
188 vesicle structure and initiates fissuring of the membrane without fully collapsing the vesicle. Divalent ions,
189 such as Ca^{2+} , adsorb on phospholipid bilayers and interact with the polar head groups of the lipids [25-
190 28]. We hypothesize that as the interactions between lipid molecules in the bilayer are disrupted upon
191 heating, the divalent ions embed themselves deeper into the bilayer to better interact with the oppositely
192 charged polar headgroups, accelerating the fissuring of the membrane. Such destabilized vesicles, when
193 mixed and agitated with coacervates, could use the coacervates as a support and wrap themselves around

194 them, analogous to the rupture and fusion of GUVs on solid surfaces to form supported lipid bilayers [19].
195 When the coacervate-adsorbed membrane fragments remain sufficiently mobile, membrane fragments
196 can merge into larger intact membrane sheets, and the membrane may ultimately reseal forming
197 membrane-enclosed coacervates or membranized coacervates (MCs). Figure 1 is a schematic
198 representation of the MC formation process.

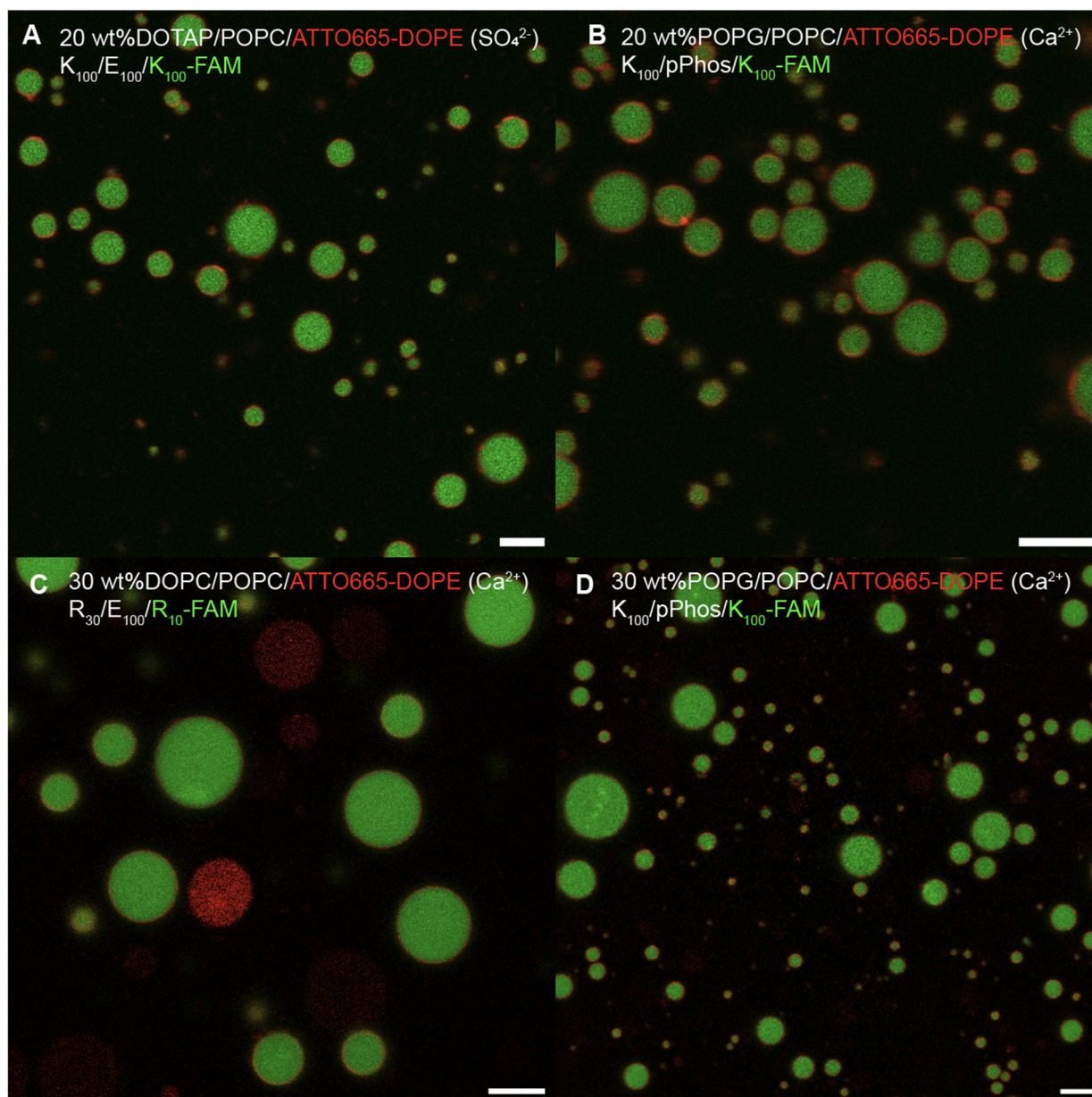


199 **Figure 1:** Schematic representation of the process of membranized coacervate formation. In the confocal images,
200 scale bar = 5 μm .

201
202 We tested this hypothesis by exposing GUVs to a carefully tuned heat shock at 60°C in the presence of
203 divalent ions (Ca^{2+} , SO_4^{2-} at a concentration of 2 mM) of the opposite charge as that of the membrane, or
204 Ca^{2+} in the case of an uncharged membrane. We then removed the heat source and mixed the GUVs with
205 a coacervate dispersion, forming membranized coacervates. Analysis of the size distributions of the
206 coacervates, GUVs and MCs supports our hypothesis in Figure 1 that the coacervates act as supporting or
207 templating surface for the adsorption and fusion of membrane fragments. The size distributions of the
208 MCs and the original coacervates are the same, and significantly different from that of GUVs (Figure S1).

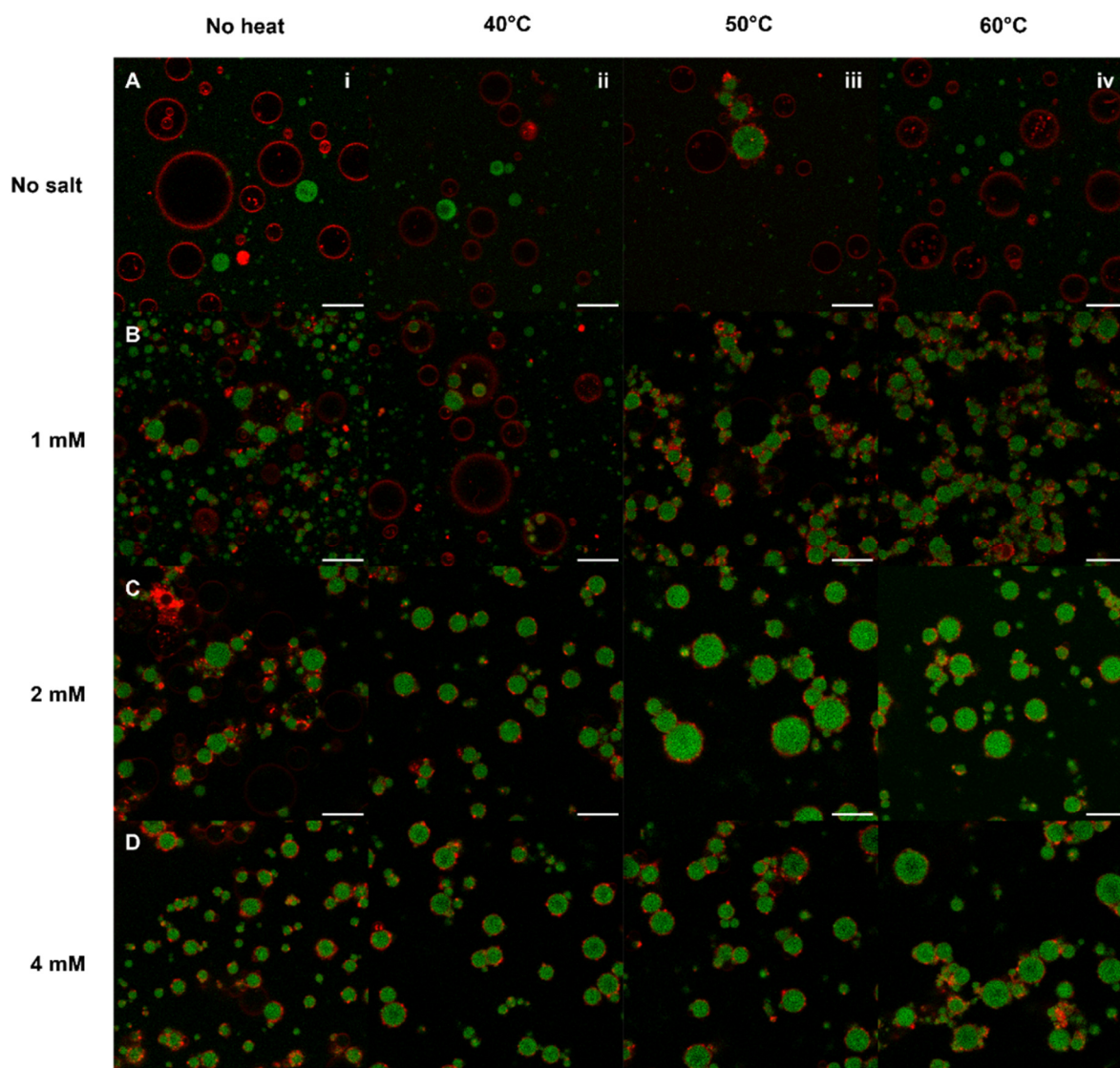
209 We tested the robustness and versatility of this method to create MCs using multiple coacervate
210 and membrane combinations (Supplementary Table 1) and found that it yielded MCs for all the tested
211 combinations, including coacervates and GUVs with very small or no surface charge, and coacervates and
212 GUVs of the same surface charge. This versatility provides flexibility in choosing the best coacervate-
213 membrane system for downstream application. We imaged the MCs using confocal fluorescence
214 microscopy, shown in Figure 2. It is of particular interest that this method also worked for similarly charged
215 coacervates and GUVs. For example, coacervates formed with poly-DL-lysine (K_{100}) and polyphosphate
216 (pPhos) have a high negative surface charge [29]. If these coacervates are mixed with POPG/POPC GUVs,
217 which also have a net negative charge, the two systems do not interact with each other (as seen in Figure
218 3A(i)). But heating the POPG/POPC GUVs in the presence of 2 mM Ca^{2+} , and then cooling and mixing them
219 with K_{100} /pPhos coacervates results in the negatively charged GUVs wrapping around the negatively
220 charged coacervates, forming stable MCs. In such cases, the divalent ions also help screening the surface
221 charge apart from facilitating membrane fissioning.

222 To support our hypothesis of the role of temperature and divalent ions in GUV destabilization, we
223 tried making MCs by heating the GUVs at 40°C, 50 °C, and 60 °C with 1 mM, 2 mM, 4 mM or no divalent
224 ions before mixing them with the coacervates. We observed that MCs formed best when GUVs were



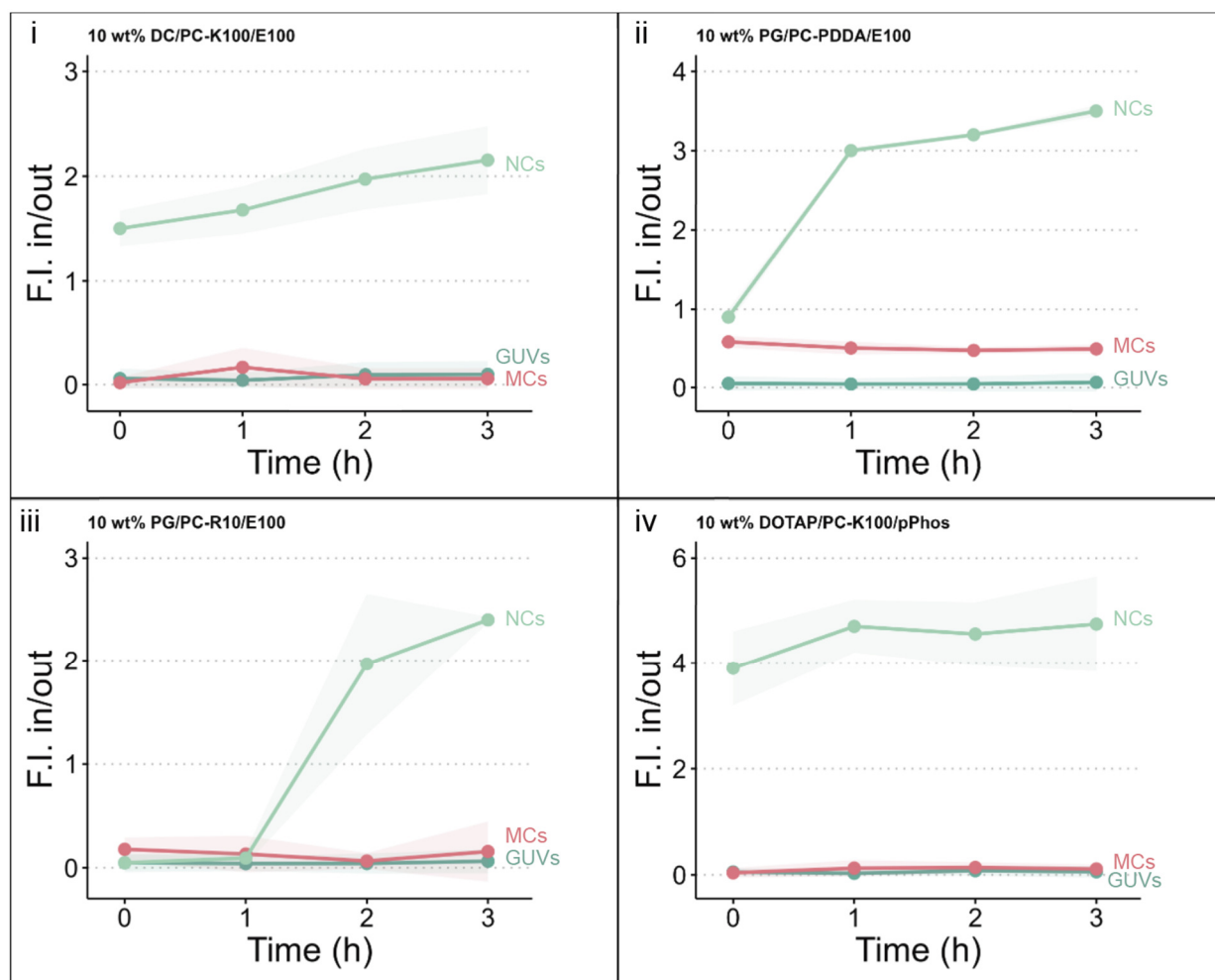
225
 226 **Figure 2: Representative images of membranized coacervates (MCs) formed with different coacervate and GUVs.**
 227 All GUVs were labelled with ATTO665-DOPE. Images show MCs formed with A) 20 wt% DOTAP/POPC GUVs and
 228 $K_{100}/E_{100}/K_{100}$ -FAM coacervates in presence of SO_4^{2-} , B) 20 wt% POPG/POPC GUVs and $K_{100}/pPhos/K_{100}$ -FAM
 229 coacervates in presence of Ca^{2+} , C) 30 wt% DOPC/POPC GUVs and $R_{30}/E_{100}/R_{10}$ -FAM coacervates in presence of Ca^{2+} ,
 230 and D) 30 wt% POPG/POPC GUVs and $K_{100}/pPhos/K_{100}$ -FAM coacervates in presence of Ca^{2+} . Scale bar = 5 μm .

231
 232
 233 heated at temperatures above 50 °C with 2 mM of divalent ion salt (Figure 3). A higher salt concentration
 234 of 4 mM also yielded MCs, even at lower temperatures, however, the formed MCs often agglomerated
 235 into large clusters. We also tried to create MCs in presence of 4 mM, 8 mM, and 16 mM NaCl. If divalent
 236 ions were only necessary for charge screening (in case of similarly charged coacervates and GUVs), then
 237 monovalent ions at equivalent ionic strength should also facilitate MC formation. However, we did not
 238 observe MCs after heating the GUVs with NaCl and mixing them with the coacervates (Figure S2).



239
 240 **Figure 3: Membranized coacervates form best at temperatures above 50 °C with 2 mM of divalent ions.** The images
 241 show MC formation with 20 wt%POPG/POPC GUVs and K₁₀₀/pPhos/K₁₀₀-FAM coacervates at 20 °C, 40 °C, 50 °C, or
 242 60 °C, in the presence of 0 mM, 1 mM, 2 mM, or 4 mM Ca²⁺. Without heating the GUVs or in the absence of Ca²⁺,
 243 we do not see much interaction between the GUVs and the coacervates. MC formation requires destabilization of
 244 GUVs at temperatures above 50 °C in presence of at least 2 mM of divalent ions.

245
 246 **3.2 Properties of the MC membranes**
 247 *3.2.1 MC membranes form a selective barrier*
 248 Confocal microscopy images of MCs indicated that there is a continuous membrane around the coacervates.
 249 However, we wanted proof that the membrane forms a selective barrier between the inner coacervate
 250 phase and the outer dilute phase. To test the permeability of the membrane, we monitored the diffusion of
 251 calcein and 5-TAMRA (both used at a final concentration of 2 mM) across the MC membrane and compared
 252 it with their diffusion across GUVs and bare coacervates of the same composition. Coacervates, due to their
 253 lesser water content (or reduced polarity) compared to the surrounding dilute aqueous phase, have high
 254 affinity for hydrophobic molecules [30]. This means, that if the membrane around the coacervate is not
 255 continuous, most fluorescent dyes will rapidly partition inside the coacervate.



256

257 **Figure 4: Membranized coacervate membranes form a selective barrier, keeping small molecules out similar to**
 258 **GUV membranes.** The plots show ratios of fluorescence intensities inside GUVs, MCs, and naked coacervates (NCs)
 259 over that in solution for calcein (i, ii, and iii) and 5-TAMRA (iv) over time.

260

261 As expected, the dyes swiftly partitioned inside the naked coacervates (NCs), resulting in high
 262 fluorescence intensity inside the coacervate compared to the outside. By contrast, the MC membranes
 263 kept the small molecules out and the fluorescence intensity in the coacervate interior remained low
 264 similar to that in the GUV lumen. Figure 4 shows the increase in the ratio of fluorescence intensities inside
 265 the GUVs, naked coacervates, and MCs over outside with time. The ratio remained nearly constant for
 266 more than 3 hours, indicating that the MCs did not take up the dyes over time. In case of MCs formed
 267 with 10 wt% POPG/POPC GUVs and PDDA/ATP coacervates (Figure 4(ii)), the fluorescence intensity ratio
 268 is slightly larger than that for the corresponding GUVs but remains constant over time. This could be
 269 because the membrane fragments around the coacervate took longer to close the gaps between each
 270 other and some calcein diffused inside the coacervates before all the gaps could seal. Once the membrane
 271 fragments merged into a continuous membrane, the diffusion of calcein stopped and the fluorescence
 272 intensity ratio in/out stayed constant over time. Hence, the membranes around the MCs are continuous
 273 and form a selective barrier.

274 3.2.2 MCs are resilient to fluctuations in the external environment

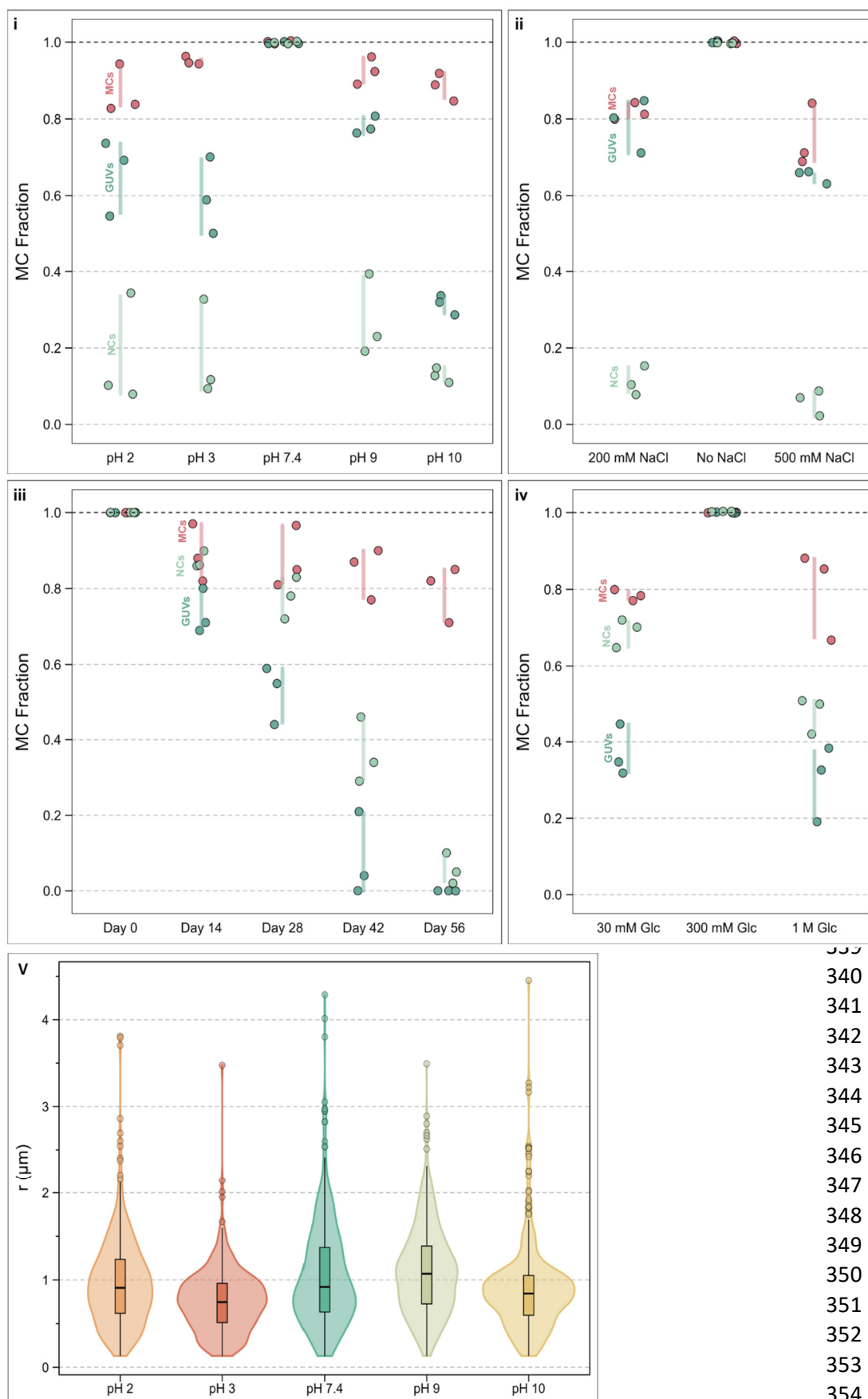
275 Protocells must have needed to remain stable or viable under a range of environmentally changing
276 conditions to survive and evolve. Vesicles and coacervates have different strengths and weaknesses—the
277 former are prone to bursting or collapsing under osmotic stress, while the latter are sensitive to high salt
278 concentrations or extreme pH. We hypothesize that MCs combine the strengths of both protocell systems
279 and remain stable under a much wider range of conditions. To test this hypothesis, we subjected the MCs
280 various environmental stresses — changes in pH, osmolarity, and salt concentrations. We also tested their
281 viability over time at -20 °C and freeze-thaw cycles.

282 First, we exposed MCs, coacervates and liposomes to hyper and hypo-osmotic shocks. Liposomes
283 are sensitive to differences in osmolarities between the inner and outer solutions. In hypotonic
284 conditions, the vesicles swell and eventually burst. Under hypertonic stress, water diffuses out of the
285 vesicles making them flaccid and unstable. We subjected MCs made in 300 mM glucose solution to hyper
286 and hypo-osmotic stress by suspending them in 1 M and 30 mM glucose solutions, respectively, and
287 monitored their stability over time. Over 75% MCs retained their shape and size under hypo- and
288 hyperosmotic stress compared to the control, and remained stable over time, while liposomes of the
289 same composition fared much worse (Figure 5(i)).

290 We also tested the effect of 200 mM and 500 mM NaCl on MC stability. MCs were able to
291 withstand changing salt concentrations, whereas naked coacervates of the same composition dissolved
292 at the tested salt concentrations (Figure 5(ii)). We attribute this enhanced resilience to changes in salt
293 concentration to the continuous membrane surrounding the coacervates. If the MC membrane was not
294 continuous and had pores in it, the salt ions would be able to enter the inner coacervate, disrupt the
295 electrostatic interactions between the coacervate polymers, and visibly cause its dissolution.

296 Next, we next tested the resilience of MCs to changes in pH. Most complex coacervates contain
297 components that can be protonated or deprotonated in acidic or basic conditions. When formed in buffer-
298 less solutions at physiological pH (7.3-7.4), these coacervates cannot withstand large pH fluctuations. pH
299 fluctuations can also deform or induce chemical polarization in lipid vesicles and lead to bursting [31]. We
300 exposed MCs made from K₁₀₀/pPhos coacervates and 20 wt% POPG/POPC GUVs to pH 2, 3, 9, and 10 by
301 adding 0.1 M HCl or 0.1 M NaOH to the solution and monitored their structural integrity over time in
302 comparison to the same MCs at pH 7.3 (control). Figure 5(iii) shows that MCs weathered the stresses due
303 to pH variations well with more than 70% of them surviving most conditions.

304 Finally, MCs need to be able to withstand multiple freeze-thaw cycles over long time periods. To
305 test their resilience to freeze-thaw cycles, we stored MCs in an eppendorf at -20 °C, thawed them every
306 two weeks for eight weeks, and assessed their number and morphology. More than 90% of MCs remained
307 intact over a period of eight weeks (Figure 5(iv)). We did not observe visible changes in the MC
308 morphology. Moreover, the size distribution of MCs does not vary widely under different conditions,



355 **Figure 5: MCs are more resilient to environmental fluctuations compared to GUVs and coacervates.** The plots show
 356 the fraction of MCs, GUVs, and naked coacervates (NCs) that survived under changing pH (i), increasing salt
 357 concentrations (ii), through freeze-thaw cycles (iii), and osmotic stress (iv) compared to the MCs in the optimal
 358 solution conditions (MC fraction = 1). MC size distribution in different pH (v).

359 further indicating their stability (Figure 5(v), S3). By contrast, less than 10% of bare coacervates and
360 liposomes was still intact after eight weeks of freeze-thaw cycles. Our results indicate that MCs are much
361 more stable than their constituent species and can withstand drastic changes in the external environment.
362 These features make MCs an ideal protocell model and synthetic cell compartment to encapsulate and
363 store molecules for extended periods, carry out reactions and host complex reactions networks in a well
364 closed-off and distinct environment.

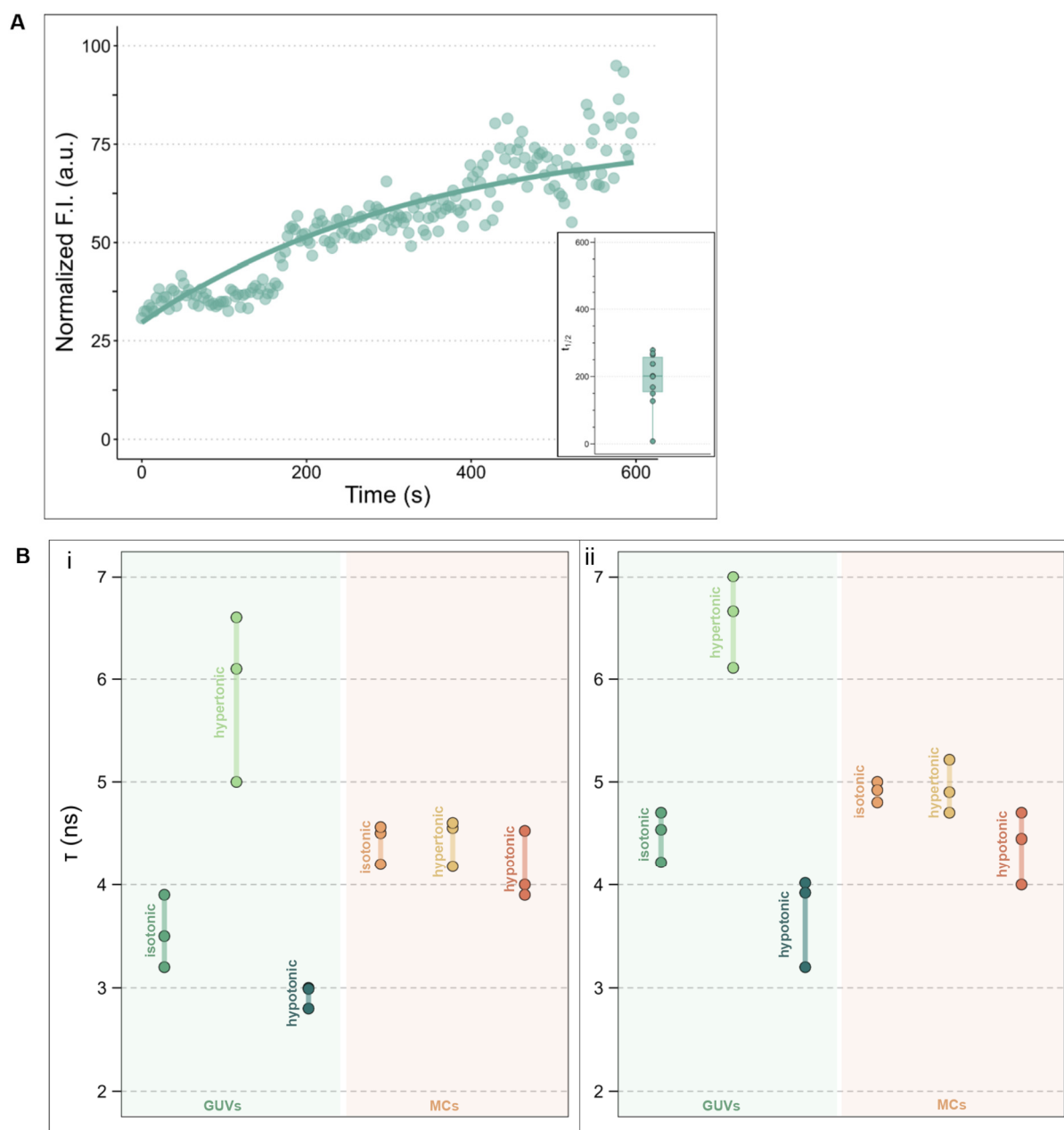
365

366 *3.2.3 Lipids in MC membranes are mobile but densely packed*

367 We also monitored the fluorescence recovery after photobleaching (FRAP) to determine the mobility of
368 the lipids in the MC membranes. The ease of lipid diffusion across the membrane also gives an idea about
369 the membrane continuity. If the lipid bilayer is discontinuous or the lipids are adsorbed on the surface of
370 the coacervates without forming a well-defined bilayer, then lateral diffusion of the lipids will be slow or
371 nearly absent and we will see little to no fluorescence recovery. Figure 6A shows a representative FRAP
372 curve and the half-time of recovery ($t_{1/2}$) we obtained for our MCs (n=10). Most MC membranes showed
373 a fluorescence recovery of about 70% of the pre-bleach levels, indicating that the lipids in the MC
374 membranes remain mobile.

375 Finally, we also assessed the lipid packing within the MC membranes by monitoring the changes
376 in the fluorescence lifetime (τ) of an environment-sensitive probe, FliptR [32], using fluorescence lifetime
377 imaging microscopy (FLIM) in GUV and MC membranes of the same composition. In membranes with
378 high surface tension, loose lipid packing, or low cholesterol content (fluid membranes), FliptR has shorter
379 τ as the rotor molecule largely exists in a non-planar form [32]. However, in membranes with low surface
380 tension, denser lipid packing, or high cholesterol content (rigid membranes), the molecule is sterically
381 hindered and exists in its planar form with longer τ .

382 We subjected GUVs and MCs with the same membrane composition to hyper and hypoosmotic
383 conditions and measured the fluctuations in FliptR τ (Figure 6B). We used 20 wt%POPG/POPC GUVs with
384 10 wt% (Figure 6B(i)) and 20 wt% (Figure 6B(ii)) cholesterol. As expected, FliptR in membranes with 20
385 wt% cholesterol had longer τ values compared with that in membranes with 10 wt% cholesterol. In the
386 case of GUVs, the τ values varied depending on the solution osmolarity, indicating that the surface tension
387 of the GUV membrane fluctuates and is largely dependent on the external environment. On the other
388 hand, the τ values did not vary so much for MCs in isotonic, hypertonic, or hypotonic conditions. This
389 indicates that MC membranes are stable against osmotic changes, likely due to the support of and
390 interaction with the coacervate interior. Moreover, MC membranes seem to have a denser lipid packing
391 compared to their GUVs counterparts as indicated by the longer τ values for MCs in isotonic conditions
392 compared with that of GUVs of the same composition.



393 **Figure 6: Properties of the MC membranes.** A) A representative fluorescence recovery curve of an ROI in an MC
 394 membrane; the inset shows the half times of fluorescence recovery for ROI in $n=10$ MC membranes. B) FliptR
 395 fluorescence lifetimes in GUV and MC membranes containing 10 wt% (i) or 20 wt% (ii) cholesterol in isotonic,
 396 hypertonic, and hypotonic conditions.

397

398

399 4. Conclusion

400

401 While coacervates and liposomes can mimic certain components of modern cells—biocondensates and
 402 membrane-bound compartments, respectively—and hence have served as protocells models, neither can
 403 epitomize living cells alone. Here, we have shown a simple and robust method to create membranized
 404 coacervates with a biomolecule-rich interior delineated by a lipid membrane. MCs are more resilient

405 against changing environmental pH, osmolarity, and salt concentrations and can withstand multiple
406 freeze-thaw cycles, making their long-term storage feasible. The MC membranes are continuous, their
407 lipids more densely packed than the corresponding GUVs, and their fluidity is influenced by the inner
408 coacervate core. We can use these MCs as protocell models and study interactions and biomolecule
409 exchange between various MC populations to better understand how primitive cells might have
410 interacted and evolved. Moreover, MCs might also serve as stable and versatile cellular delivery vehicles.

411

412 **5. Author information**

413 * Correspondence: e.spruijt@science.ru.nl

414

415 **6. Acknowledgements**

416 This work was supported financially by the International Human Frontier Science Program Organization
417 (HFSP) via award RGY00062/2022. The authors acknowledge Gert-Jan Bakker (Radboudumc) for help
418 with the FLIM and FRAP measurements.

419

420 **7. Notes**

421 The authors declare no competing financial interest.

422

423 **8. References**

- 424 1. Charman, M., et al., A viral biomolecular condensate coordinates assembly of progeny particles. *Nature*, 2023.
425 616(7956): p. 332-338.
- 426 2. Liao, Y.C., et al., RNA Granules Hitchhike on Lysosomes for Long-Distance Transport, Using Annexin A11 as a
427 Molecular Tether. *Cell*, 2019. 179(1): p. 147-164.e20.
- 428 3. Su, X., et al., Phase separation of signaling molecules promotes T cell receptor signal transduction. *Science*, 2016.
429 352(6285): p. 595-599.
- 430 4. Fujioka, Y., et al., Phase separation organizes the site of autophagosome formation. *Nature*, 2020. 578(7794): p.
431 301-305.
- 432 5. Bussi, C., et al., Stress granules plug and stabilize damaged endolysosomal membranes. *Nature*, 2023. 623(7989):
433 p. 1062-1069.
- 434 6. Yewdall, N.A.-O., A.A.-O. Mason, and J.A.-O. van Hest, The hallmarks of living systems: towards creating artificial
435 cells. *Interface focus*, 2018. 8(5).
- 436 7. Slootbeek, A.A.-O.X., et al., Growth, replication and division enable evolution of coacervate protocells. *Chemical*
437 *communications*, 2022. 58(80): p. 11183-11200.
- 438 8. Gilbert, W., Origin of life: The RNA world. *Nature*, 1986. 319(6055): p. 618-618.
- 439 9. Segré, D., et al., The lipid world. *The journal of the International Society for the Study of the Origin of Life*, 2001.
440 31(1-2): p. 119-145.
- 441 10. Yarus, M., Getting past the RNA world: the initial Darwinian ancestor. LID - 10.1101/cshperspect.a003590 [doi]
442 LID - a003590. *Cold Spring Harbor perspectives in biology*, 2011. 3(4).
- 443 11. Hunding, A., et al., Compositional complementarity and prebiotic ecology in the origin of life. *BioEssays : news*
444 *and reviews in molecular, cellular and developmental biology*, 2006. 28(4): p. 399-412.
- 445 12. Kusumaatmaja, H.A.-O., et al., Wetting of phase-separated droplets on plant vacuole membranes leads to a
446 competition between tonoplast budding and nanotube formation. LID - 10.1073/pnas.2024109118 [doi] LID

- 447 - e2024109118. Proceedings of the National Academy of Sciences of the United States of America, 2021.
448 118(36).
- 449 13. Mangiarotti, A.A.-O., et al., Wetting and complex remodeling of membranes by biomolecular condensates.
450 Nature communications, 2023. 14(1).
- 451 14. Mangiarotti, A.A.-O., et al., Biomolecular condensates modulate membrane lipid packing and hydration. Nature
452 communications, 2023. 14(1).
- 453 15. Lu, T., et al., Structure-Property Relationships Governing Membrane-Penetrating Behaviour of Complex
454 Coacervates. Small (Weinheim an der Bergstrasse, Germany), 2023. 19(38).
- 455 16. Pir Cakmak, F., A.T. Grigas, and C.A.-O. Keating, Lipid Vesicle-Coated Complex Coacervates. Langmuir : the ACS
456 journal of surfaces and colloids, 2019. 35(24): p. 7830-7840.
- 457 17. Pir Cakmak, F., A.M. Marianelli, and C.A.-O. Keating, Phospholipid Membrane Formation Templated by
458 Coacervate Droplets. Langmuir : the ACS journal of surfaces and colloids, 2021. 37(34): p. 10366-10375.
- 459 18. Gao, N.A.-O. and S.A.-O. Mann, Membranized Coacervate Microdroplets: from Versatile Protocell Models to
460 Cytomimetic Materials. Accounts of chemical research, 2023. 56(3): p. 297-307.
- 461 19. Hardy, G.J., R. Nayak, and S. Zauscher, Model cell membranes: Techniques to form complex biomimetic
462 supported lipid bilayers via vesicle fusion. Current Opinion in Colloid & Interface Science, 2013. 18(5): p. 448-
463 458.
- 464 20. Tsugane, M. and H. Suzuki, Elucidating the Membrane Dynamics and Encapsulation Mechanism of Large DNA
465 Molecules Under Molecular Crowding Conditions Using Giant Unilamellar Vesicles. ACS Synthetic Biology,
466 2020. 9(10): p. 2819-2827.
- 467 21. Kenworthy, A.K., Fluorescence Recovery After Photobleaching Studies of Lipid Rafts, in Lipid Rafts, T.J. McIntosh,
468 Editor. 2007, Humana Totowa, NJ.
- 469 22. Kohze, R., et al., Frapbot: An open-source application for FRAP data. Cytometry Part A, 2017. 91(8): p. 810-814.
- 470 23. Warren, S.C., et al., Rapid Global Fitting of Large Fluorescence Lifetime Imaging Microscopy Datasets. PLOS ONE,
471 2013. 8(8): p. e70687.
- 472 24. Pau, G., et al., EBImage—an R package for image processing with applications to cellular phenotypes.
473 Bioinformatics, 2010. 26(7): p. 979-981.
- 474 25. McLaughlin S Fau - Mulrine, N., et al., Adsorption of divalent cations to bilayer membranes containing
475 phosphatidylserine. The Journal of general physiology, 1981. 77(4): p. 445-473.
- 476 26. Clarke, R.J. and C. Lüpfer, Influence of anions and cations on the dipole potential of phosphatidylcholine vesicles:
477 a basis for the Hofmeister effect. Biophysical journal, 1999. 76(5): p. 2614-2624.
- 478 27. Böckmann, R.A. and H. Grubmüller, Multistep binding of divalent cations to phospholipid bilayers: a molecular
479 dynamics study. Angewandte Chemie (International ed. in English), 2004. 43(8): p. 1021-1024.
- 480 28. Yang, J., et al., Specific Ion Binding at Phospholipid Membrane Surfaces. Journal of Chemical Theory and
481 Computation, 2015. 11(9): p. 4495-4499.
- 482 29. van Haren, M.H.I., B.S. Visser, and E. Spruijt, Probing the surface charge of condensates using
483 microelectrophoresis. Nature Communications, 2024. 15(1): p. 3564.
- 484 30. Lin, Z., et al., Coacervate Droplets for Synthetic Cells. Small methods, 2023. 7(12).
- 485 31. Angelova, M.I., et al., pH sensing by lipids in membranes: The fundamentals of pH-driven migration, polarization
486 and deformations of lipid bilayer assemblies. Biochimica et biophysica acta. Biomembranes, 2018. 1860(10):
487 p. 2042-2063.
- 488 32. Colom, A., et al., A fluorescent membrane tension probe. Nature Chemistry, 2018. 10(11): p. 1118-1125.

Supplementary Information

Spontaneous wrapping of coacervates by lipid bilayers upon heat shock creates resilient and intact membranized coacervates

Sadaf Javed¹, Evan Spruijt¹

¹*Institute for Molecules and Materials, Radboud University, Heyendaalseweg 135, 6525 AJ, Nijmegen, The Netherlands*

Supplementary Table 1: GUVs and coacervates used to create membranized coacervates and their mixing charge concentration ratios.

GUV composition	Coacervate composition		
	Polyanion	Polycation	Mixing [charge] ratio
30wt% DOPC/POPC	Poly-DL-Glutamate (x=100)	Polyarginine (x=30)	1:1
30wt% POPG/POPC	Hexametaphosphate	Poly-DL-Lysine (x=100)	1:1 1:1.5
10wt% DOPC/POPC	Poly-DL-Glutamate (x=100)	Poly-DL-Lysine (x=100)	1.5:1
10wt% DOTAP/POPC	Poly-DL-Glutamate (x=100)	PDDA	1:1
10wt% POPG/POPC	Poly(uridylic acid) (x=15)	Poly-DL-Lysine (x=100)	1:1
30wt% DOPC/POPC	ATP	PDDA	2:1
10wt% DOTAP/POPC	Hexametaphosphate	Poly-DL-Lysine (x=100)	1:1
30wt% DOTAP/POPC	Poly-DL-Glutamate (x=100)	Polyarginine (x=30)	1:1
30wt% POPG/POPC	Poly-DL-Glutamate (x=100)	Polyarginine (x=30)	1:1
20wt% DOTAP/POPC	Poly-DL-Glutamate (x=100)	(RGRGG) ₅	1:1

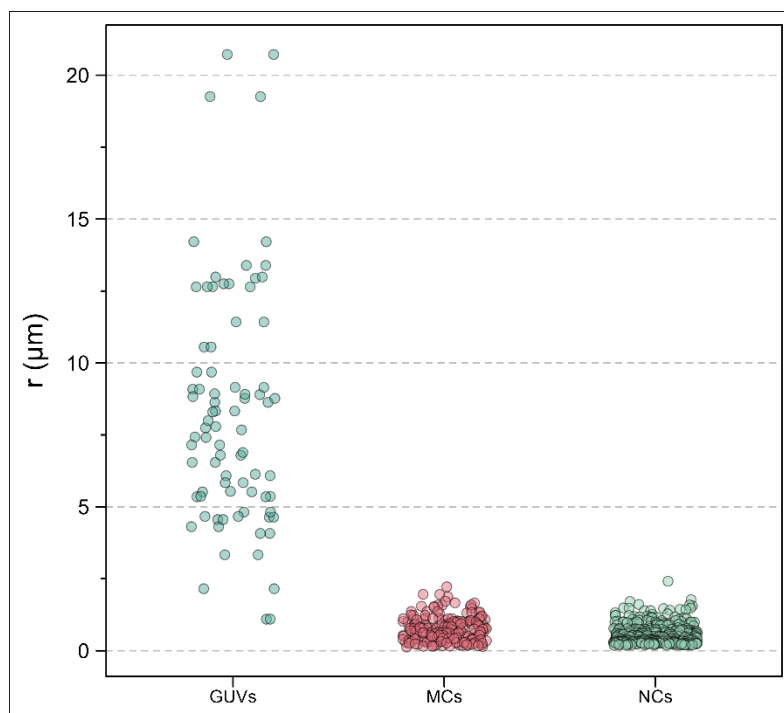


Figure S1: Size comparison for GUVs, MCs, and coacervates. MC sizes are more comparable to those of coacervates than those of the GUVs.

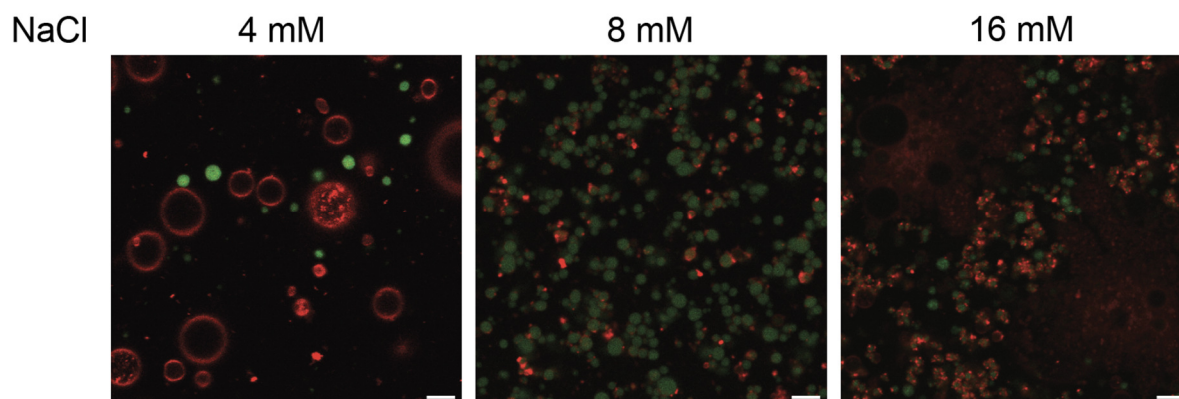


Figure S2: GUV membranes do not wrap around the coacervates in the presence of monovalent ions. The images show 20 wt%POPG/POPC GUVs and $K_{100}/pPhos/K_{100}$ -FAM coacervates. There was no interaction between the coacervates and the GUVs after heating the GUVs at 60 °C in presence of 4 mM, 8 mM, or 16 mM NaCl. In presence of 16 mM NaCl, many GUVs burst, and the lipids spread on the microscopy slide instead of wrapping around the coacervates.

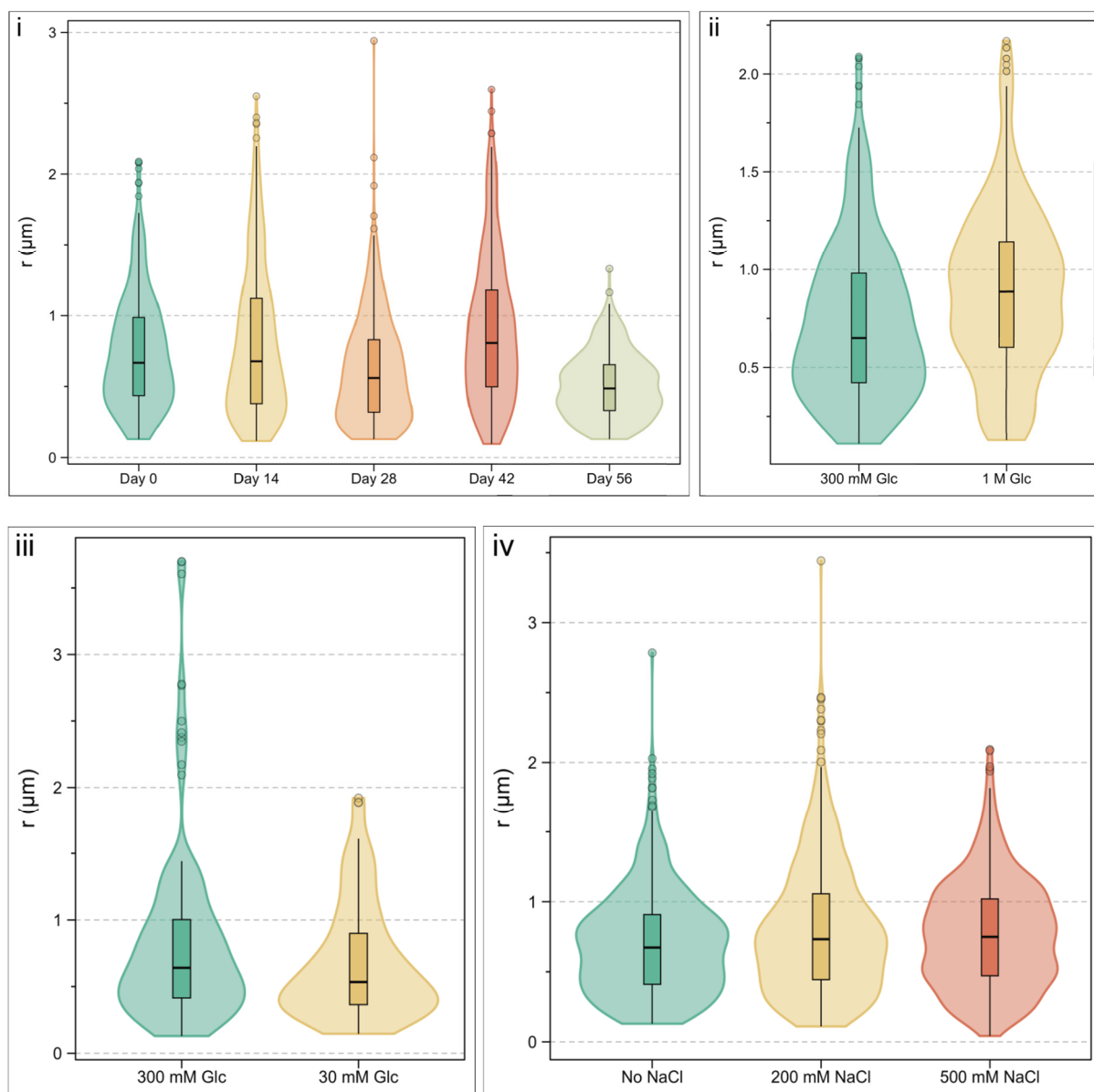


Figure S3: MC size distribution under different conditions. Size distribution of 20 wt% POPG/POPC-K₁₀₀/pPhos MCs after freeze-thaw cycles over 56 days (i), under hyper (ii) and hyposmotic stress (iii), and in 200 mM and 500 mM NaCl solutions (iv).